Available online at www.sciencedirect.com
ScienceDirect
Acta Materialia 57 (2009) 1586–1601
Acta MATERIALIA
www.elsevier.com/locate/actamat

Microstructural evolution and mechanical properties of Cu–Al alloys subjected to equal channel angular pressing

S. Qu [a], X.H. An [a,*], H.J. Yang [a], C.X. Huang [a], G. Yang [b], Q.S. Zang [a], Z.G. Wang [a], S.D. Wu [a,*], Z.F. Zhang [a,*]

[a] *Shenyang National Laboratory for Materials Science, Institute of Metal Research, Chinese Academy of Sciences, 72 Wenhua Road, Shenyang 110016, China*
[b] *Central Iron and Steel Research Institute, Beijing 100081, China*

Received 7 October 2008; received in revised form 2 December 2008; accepted 2 December 2008
Available online 3 January 2009

Abstract

Ultrafine-grained (UFG) or nanocrystalline (NC) Cu–Al alloys were prepared using equal-channel angular pressing (ECAP) to investigate the influence of stacking fault energy (SFE) on the microstructural evolution during deformation and the corresponding mechanical properties. The grain refinement mechanism was gradually transformed from dislocation subdivision to twin fragmentation by tailoring the SFE of alloys. Meanwhile, homogeneous microstructures and nanoscale grains were readily achieved in the low-SFE Cu–Al alloys and the equilibrium grain size was decreased by lowering the SFE. Moreover, in the Cu–Al alloy with extremely low SFE, shear fracture occurred during ECAP at strain levels higher than two due to the formation of macroscopic shear bands. In addition, the normalized deformation conditions at large strain were qualitatively discussed. More significantly, the strength and uniform elongation were simultaneously improved by lowering the SFE. This simultaneity results from the formation of profuse deformation twins and microscale shear bands, and their extensive intersections.

Keywords: Cu–Al alloys; Stacking fault energy (SFE); Equal channel angular pressing (ECAP); Strength; Ductility

1. Introduction

Over the past decade, substantial grain refinement from the micrometer to the sub-micrometer or nanometer level through the application of severe plastic deformation (SPD) [1] has attracted considerable attention due to its potential to significantly enhance the mechanical properties of materials. Various techniques based on SPD, such as equal-channel angular pressing (ECAP) [2–7], high-pressure torsion (HPT) [8,9], accumulative roll bonding [10], ball milling (BM) [11], surface mechanical attrition treatment (SMAT) [12,13] and dynamic plastic deformation (DPD) [14,15], have been widely developed to produce ultrafine-grained (UFG) or nanocrystalline (NC) materials, reaping remarkable improvements in the mechanical properties. Of these various processes, ECAP is the most versatile processing technique used to fabricate large billets of bulk, dense and contamination-free UFG materials that can be used in a wide range of structural applications. Since the cross-section geometry is unchanged after pressing, repetitive pressings and different routines can be easily performed in the same sample. Thus, this technique can provide sufficiently high strain to harvest fairly homogeneous microstructures and extensively refined grains [2].

It has been well-documented that the microstructural evolution and grain refinement during ECAP generally originate from various dislocation activities in the metals with medium or high stacking fault energy (SFE), e.g. Al, Cu, Fe, Ni [3–7,16,17]. Previous studies indicate that grain refinement is predominately operated by accumulation,

* Corresponding authors.
E-mail addresses: xhan@imr.ac.cn (X.H. An), shdwu@imr.ac.cn (S.D. Wu), Zhfzhang@imr.ac.cn (Z.F. Zhang).

1359-6454/$34.00 © 2008 Acta Materialia Inc. Published by Elsevier Ltd. All rights reserved.
doi:10.1016/j.actamat.2008.12.002

interaction, tangling and spatial rearrangement of dislocations. At low strain levels, each grain is divided into many volume elements on account of the differences in the number and selections of active slip systems. These volume elements are separated by geometrically necessary boundaries (GNBs) and incidental dislocation boundaries (IDBs) within the grains. Further plastic strain will increase the misorientations of GNBs and IDBs leading to the formation of high-angle grain boundaries, as well as smaller grains inside the original coarse grains. This is the well-known dislocation subdivision mechanism [1–4]. With increasing degree of deformation, however, rather than grain refinement, the most pronounced microstructural change is an increment in the portion of high-angle grain boundaries. Typically, the equilibrium grain size obtained via the dislocation subdivision mechanism is not within the nanometer scale (<100 nm) but in the UFG range (100 nm–1 μm). For example, the limiting grain size of Al [3,4,18] is about 0.5–1.5 μm, while for Cu [5,18] and Fe [16], the minimum grain sizes are in the range of 200–300 nm. The limitation of grain refinement can be attributed to the extensive dynamic recovery balancing multiplication and annihilation of dislocations, usually happened in the materials with the high-/medium-SFE. The annihilation processes are also facilitated by more interactions between dislocations and grain boundaries. Consequently, no more dislocation boundaries can be formed, hindering the further subdivision of grains.

However, nanoscale grains via plastic strain-induced refinement in these high- or medium-SFE materials (such as Cu) can be achieved by the BM, SMAT and DPD with extremely rigorous deformation conditions [11–15]. By restricting the dislocation motion in these methods, deformation twinning, a prominent deformation mechanism in low-SFE materials, plays a crucial role in grain refinement [19,20]. Therefore, it is reasonable to expect that the grain size can also be refined down to the nanoscale for metals with low SFE even under relatively gentle deformation conditions. For example, the minimum grain size is about 10 nm in Cu–30% Zn processed by HPT [21,22], and 31 nm for austenite and 74 nm for martensite in austenitic stainless steel by ECAP [23]. In practice, refinement via deformation twinning primarily stems from the interactions between dislocations and twin boundaries resulting in the fragmentation of twin bundles. This is the well-established twin fragmentation mechanism [12–15]. However, the transition of microstructural evolution from high-SFE metals to extremely low-SFE metals is less informed. In this work, regarding the significance of SFE in plastic deformation, we investigate the influence of SFE on the microstructure of Cu–Al alloys during the ECAP process.

With significant grain refinement, such metals typically have very high strength, several times higher than that found in their coarse-grained (CG) counterparts; unfortunately, their inadequate ductility has become an essential drawback that has limited their practical applications. As widely accepted, the ductility of metallic materials is controlled by strain hardening, which is caused by the accumulation of crystalline defects and makes further deformation harder. On the microscale, due to nearly saturated defects introduced during processing and diminished dislocation activities in ultrafine grains, these strong materials tend to lose the ability to store dislocations and the capacity for strain hardening. On the macroscale, the Consideré criterion governs the onset of localized deformation in tension:

$$\left(\frac{\partial\sigma}{\partial\varepsilon}\right)_{\dot{\varepsilon}} \leq \sigma \tag{1}$$

where σ and ε are the true stress and true strain, respectively. This well-known criterion also predicts that the as-processed UFG/NC alloys will lose the strain hardening quickly once yielding occurs, enhancing the propensity for plastic instability in the early stage of plastic deformation [24]. Accordingly, the disappointingly low tensile uniform elongation of those UFG materials is mainly imputed to this vulnerability to localized deformation/failure modes that plagues nearly all UFG and NC materials.

Despite several strategies being proposed to improve the tensile uniform elongation, the simultaneous upgrading of global mechanical properties is not readily achieved in bulk UFG/NC metals [25]. Recently, Zhao et al. [19] hypothesized that the properties of these materials can be meliorated by changing the SFE, and we have reported that the simultaneous increase in strength and ductility was achieved in Cu–Al alloys after 1-pass ECAP through the lowering of their SFE [20]. Therefore, tailoring SFE by alloy design may be a utilizable approach to upgrade the mechanical properties of UFG/NC materials. Thus, through the ECAP technique, we expect to gain a relatively homogeneous microstructure in UFG/NC Cu–Al alloys with a wide range of SFEs and critically discuss several questions in this manuscript: how does the SFE affect the microstructural evolution during ECAP? As the microstructures and refinement mechanisms in the present work and those with rigorous loading conditions mentioned above are similar [11–15], is there any relationship between them? How do the mechanical behaviors of these UFG/NC metals perform and how does the SFE influence them? These essential issues are meticulously elucidated through systematic investigation and detailed analysis.

2. Experimental procedure

With regard to the numerous investigations into the microstructural evolution of metals with high or medium SFE, three Cu–Al alloys with medium and low SFEs (Cu–5 at.% Al, 28 mJ m^{-2}; Cu–8 at.% Al, 17 mJ m^{-2}; and Cu–16 at.% Al, 6 mJ m^{-2}) were selected for this work [26]. First, the Cu–Al alloys with different Al contents were cast into ingots and then cold drawn into rods 8 mm in diameter. Before pressing, the Cu–Al alloy rods were annealed at 800 °C for 2 h to diminish the effect of mechanical processing and obtain homogeneous microstructures.

After that, the annealed CG Cu–Al alloy rods were cut into samples 45 mm in length for the ECAP process. The ECAP procedure was performed using a die fabricated from tool steel with two channels intersecting at an inner angle of 90° and an outer angle of 30°, accordingly yielding an effective strain of ~1.15 for each pass. All the rods coated with a MoS_2 lubricant were pressed at room temperature (RT) with a pressing speed of 9 mm min^{-1}. The Cu–5 at.% Al and Cu–8 at.% Al alloys were processed for 1–4 passes with route B_C (90° clockwise rotation around the sample axis between the pass), which is the most effective routine for the grain refinement [27]. However, the Cu–16 at.% Al alloy was only processed for one or two passes because it often failed by a shear fracture during the third pass.

A scanning electron microscope–electron channeling contrast (SEM–ECC; Cambridge S-360) technique was used to characterize the microstructures of the annealed CG Cu–Al alloys. The SEM–ECC micrographs in Fig. 1 reveal that the average grain size was estimated to be in the range of 100–500 μm and annealing twins with micrometer-dimension lamellae were frequently observed. After ECAP, the microstructure characterization was performed by transmission electron microscopy (TEM) on JEM-2000FXII and JEM-2010 transmission electron microscopes operated at 200 kV. Thin foils for TEM observations, cut from the *Y* plane [2] in the centers of the pressed rods using spark cutting, were first mechanically ground to about 50 μm thick and then thinned by a twin-jet polishing method in a solution of 25% phosphoric acid, 25% ethanol and 50% water with a voltage of 8–10 V at RT. Bright field images were taken on a transverse section along the ⟨1 1 0⟩ zone axis. Microstructural features of bulk samples processed by ECAP for four passes were also examined electron backscattered diffraction (EBSD) with LEO SUPRA35 SEM. Using this method, Kikuchi patterns can be obtained automatically at a step of 0.05 μm and the corresponding orientation angle resolution can be improved to about 1° when an emission field gun scanning electron microscope with a small beam spot size was used.

Tensile specimens with a dog-bone shape were cut into a gauge length of 8 mm, with a width of 2 mm and a thickness of 1 mm from the processed billets along the extrusion direction of ECAP. Tensile tests were carried out at RT with an Instron 8871 testing machine operating at a strain rate of 5×10^{-4} s^{-1} for both the CG reference material and the ECAP-processed specimens. At least two tensile tests were performed on each sample condition to substantiate the reproducibility of the stress–strain curves.

3. Experimental results

3.1. Microstructures of Cu–Al alloys after ECAP processes

3.1.1. Microstructural evolution of Cu–5 at.% Al alloy

Fig. 2 presents typical bright-field TEM micrographs of the microstructures of Cu–5 at.% Al alloy subjected to ECAP for 1–4 passes. At the initial stage of deformation, the microstructures mainly consist of strongly elongated subgrains/cells with roughly parallel lamellar boundaries, as also observed in pure Cu and Al [1,2]. These lamellar boundaries with average spacing of approximately 200–400 nm, recognized as GNBs, can accommodate the glide-induced lattice rotation in the adjoining volume. Different from the microstructures of Cu after 1-pass ECAP, a few mechanical twins can be observed in some deformed grains due to its relatively low SFE, as depicted in Fig. 2(b). After two passes, the spacing of boundaries was significantly decreased and had a mean value of ~100 nm, while several microscale shear bands (SB) formed (Fig. 2(c)). In a few zones of samples, Fig. 2(d)

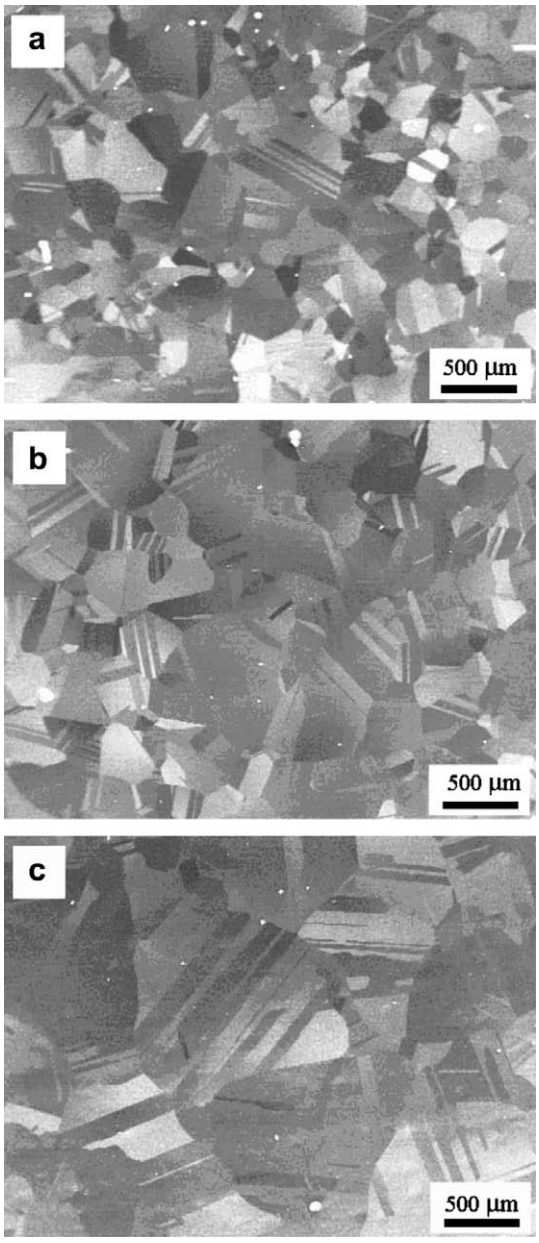

Fig. 1. SEM–ECC micrographs of annealed CG Cu–Al alloys: (a) Cu–5 at.% Al; (b) Cu–8 at.% Al; (c) Cu–16 at.% Al.

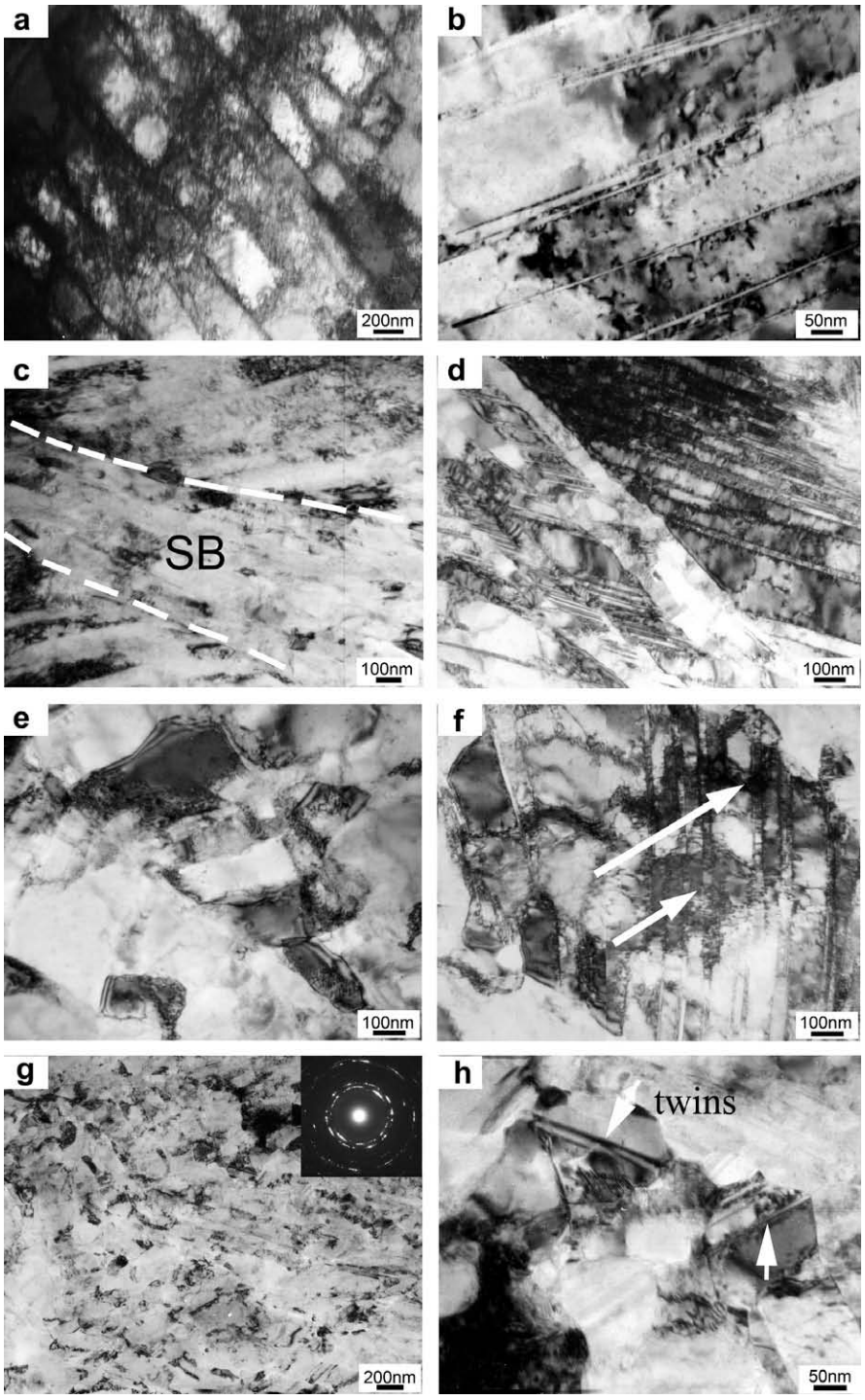

Fig. 2. Bright-field TEM images of microstructures of CG Cu–5 at.% Al alloy after ECA pressing for: (a and b) one pass; (c and d) two passes; (e and f) three passes; (g and h) four passes.

demonstrates that twin-matrix (T-M) lamellae formed, which is attributable to the decrease of SFE and favorable crystallographic orientations for twinning, and traversed the lamellar boundaries facilitating the grain refinement.

The microstructures after three passes are shown in Fig. 2(e) and (f). The fraction of the strongly elongated lamellar boundary structure essentially decreased; meanwhile, the activation of different slip systems truncated previous lamellar boundaries into approximately equiaxed subgrains, leading to a relatively homogeneous structure. As illustrated by the arrows in Fig. 2(f), extremely high-density dislocations located at the T-M lamellae imply a large stress concentration in these regions, which can help break deformation twins and refine grains with further deformation [13,14]. Thus, although the mechanism of grain refinement in Cu–5 at.% Al is still dominated by

the dislocation activities, it provides substantial evidence about the transition of refinement mechanism from the dislocation subdivision to the twin fragmentation. After four passes, the corresponding selected-area electron diffraction (SAED) pattern (Fig. 2(g)) shows large misorientations between subgrains in most areas, indicating the formation of a uniformly equiaxed subgrain structure. Meanwhile, there are a few nanosized twins in ultrafine Cu–5 at.% Al grains, as indicated in Fig. 2(h). Notwithstanding that the proportion of equiaxed subgrains is very large, the final microstructure is not consistently uniform across the whole sample. This implies that 4-passes pressing is not enough to produce a wholly homogeneous microstructure of ultrafine Cu–5 at.% Al alloy.

3.1.2. Microstructural evolution of Cu–8 at.% Al alloy

The resulting microstructures of the pressed Cu–8 at.% Al alloy for 1–4 passes are depicted in Fig. 3(a)–(h), respectively. After the first pressing, profuse thin mechanical twins with a thickness of several tens of nanometers formed in most grains, as frequently observed in Cu samples processed by SMAT [13] and DPD [14]. Our previous study showed that these thin twins and bundles are characteristic features of low-SFE Cu–Al alloys after plastic deformation and play crucial roles in strain hardening [20]. However, the twin bundles are not straight but curved gently in some regions, which can be attributed to the unique deformation mode of ECAP. During the deformation, the high-density deformation twins formed before passing through the main shear plane and then were inflected in response to the local shearing in the die. Besides the deformation twins, shear bands with a width of about 400 nm can also be observed occasionally. Unlike as-processed Cu–5 at.% Al alloy after 1-pass ECAP, no well-developed subgrains were detected in the grains where twins are evident. Fig. 3(c) and (d) reveals that, after two passes, the formation of profuse secondary twins and twin intersections leads to a finer twin network. It is interesting to find that the secondary twins are roughly perpendicular to the primary twins; this was also observed in Cu–Si alloys subjected to 1-pass ECAP and proved by the SAED pattern [28]. Apparently, the existing primary twins block the propagation of secondary twins by restricting the mean free path of the twin dislocations. In parallel, more deformation twins and extensive twin intersections form, indicating that more twinning systems have been activated to accommodate an increased shear strain. Meanwhile, similar to the scenic displayed in Fig. 2(f), high-density dislocations resided inside T-M lamellae.

Fig. 3(e) and (f) illustrates that roughly equiaxed grains formed in several areas and resultant twins can be observed frequently after three passes. However, the density of mechanical twins significantly decreased due to the fragmentation of many T-M lamellae through the complicated interactions between dislocations and twin bundles, resulting in the formation of nanograins. Fig. 3(g) confirms the formation of equiaxed nanocrystallites with random orientations in most regions after 4-pass ECAP. The corresponding SAED pattern shows a set of nearly continuous rings without any obvious preferential orientation which clearly shows the uniform distribution of misorientation between nanograins. The average grain size is approximately 82 nm, apparently lower than that of as-processed Cu–5 at.% Al, whose average grain size is about 107 nm, according to the statistical data shown in Fig. 4. In addition, the closer observation of a typical dark-field image (Fig. 3(f)) reveals the formation of nanograins inside the T-M lamellae. This convincingly validates the hypothesis that the fragmentation of twin bundles plays a decisive role in the grain refinement. More distinctly, as-processed microstructures of Cu–8 at.% Al alloy after ECAP are more homogeneous than those of Cu–5 at.% Al alloy, which may be a result of the influence of SFE on the deformation mechanism and grain refinement, and will be discussed in Section 4.1.1.

3.1.3. Microstructural evolution of Cu–16 at.% Al alloy

Fig. 5 demonstrates the microstructural evolution of the Cu–16 at.% Al alloy during ECAP processes by TEM observations. After one pass, deformation twins are evident in nearly all the grains; concurrently high-density dislocations were accumulated in the T-M lamellae. In contrast to the Cu–8 at.% Al alloy, the corresponding SAED pattern exhibits not only superposition of a couple of $\langle 0\,1\,1\rangle$ diffraction patterns which are symmetrical to each other with respect to the $\{1\,1\,1\}$ plane, indicative of a typical twin relationship, but also several streaks proving that there are many stacking faults (SFs) inside the T-M lamellae, as observed in Fig. 5(a). Aside from the formation of profuse SFs and mechanical twins, the secondary twins were also frequently observed in the as-processed Cu–16 at.% Al alloy (see Fig. 5(b)). In addition, in the high-density twin bundle regions, a number of microscale shear bands formed and their density was much higher than that in Cu–8 at.% Al alloy subjected to the same strain. Moreover, the SAED pattern confirms that some subgrains with an average transverse size of several hundreds of nanometers formed inside these bands, as displayed in Fig. 5(c). Thus, besides the high density of twins, the formation of vast SFs and microscale shear bands can help carry the severe plastic deformation in Cu–16 at.% Al alloy with extremely low SFE.

Typical bright-field TEM images of microstructures in Cu–16 at.% Al alloy after 2-pass ECAP process are exhibited in Fig. 5(d)–(f). In many zones, more mechanical twins and SFs were apparently detected with increased plastic strain, as displayed in Fig. 5(d). Furthermore, the density of microscale shear bands was increased greatly and previously formed shear bands grew quickly with a transverse size from 1.3 to 4.3 μm. Additionally, closer observation revealed that the microstructures in these larger shear bands are characterized by nanoscale equiaxed grains with an average size of approximately 50 nm. The corresponding SAED pattern indicates that the nanograins are uniformly distributed in these bands. Differing from the two previous Cu–Al alloys, the Cu–16 at.% Al alloy was often

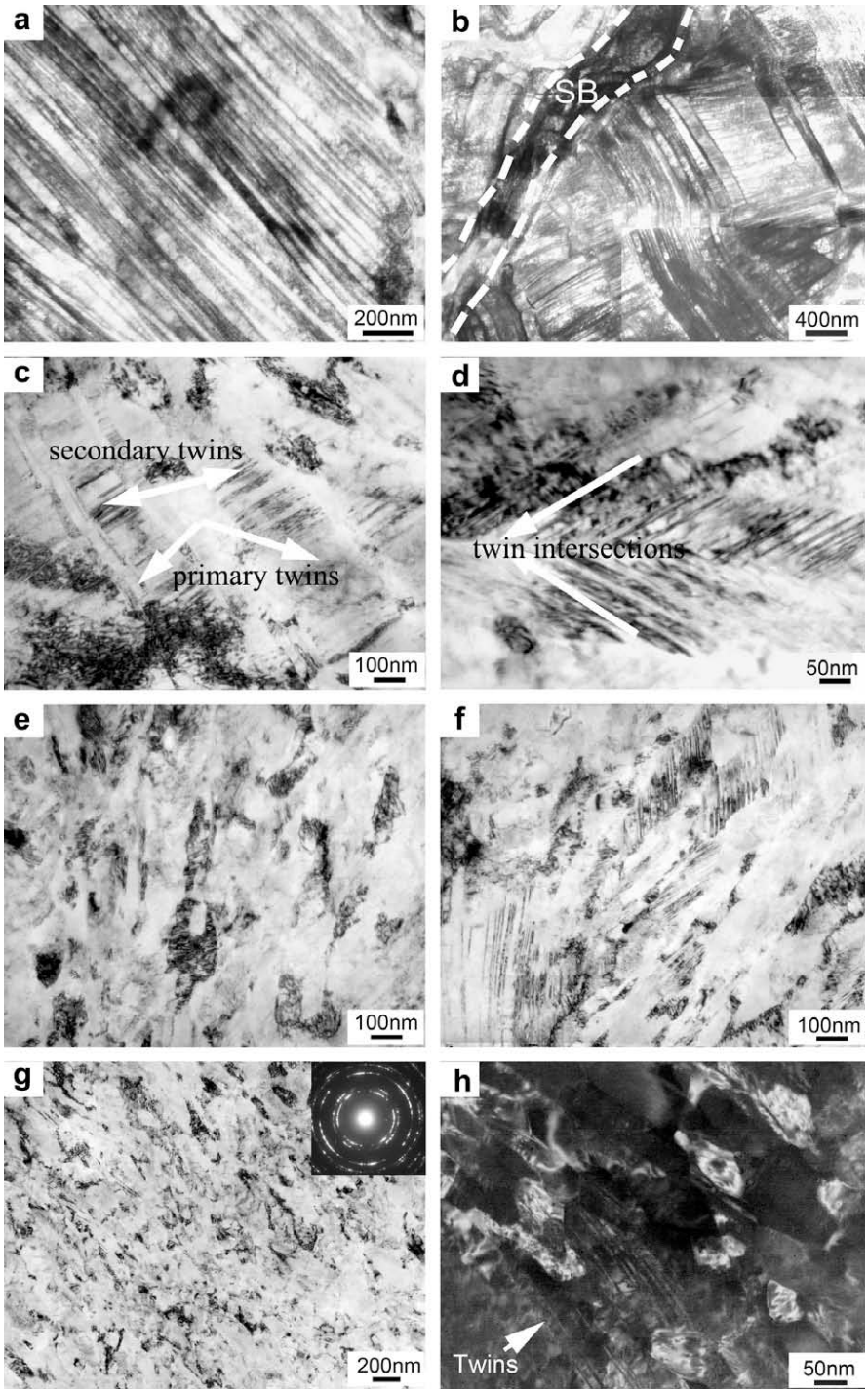

Fig. 3. TEM micrographs of microstructures of CG Cu–8 at.% Al alloy after ECA pressing for: (a and b) one pass; (c and d) two passes; (e and f) three passes; (g and h) four passes.

broken by a number of visible shear cracks when subjected to multiple-pass ECAP, as mentioned in Section 2 and this will be further discussed in Section 4.1.2.

3.2. EBSD characterization of Cu–Al alloys after 4-pass ECAP

In order to characterize the homogeneity of the post-deformation microstructure on a larger scale, the advanced EBSD technique was used to investigate the morphology, grain size and misorientation distributions of Cu–5 at.% Al and Cu–8 at.% Al alloys after ECAP for four passes. From the corresponding EBSD images in Fig. 6(a) and (b), it can be seen that the final refinement results are significantly distinct from each other due to their different refinement mechanisms. The microstructure of the ECAPed Cu–5 at.% Al alloy consists mainly of equiaxed and elongated grains, and is less homogeneous than that of the processed

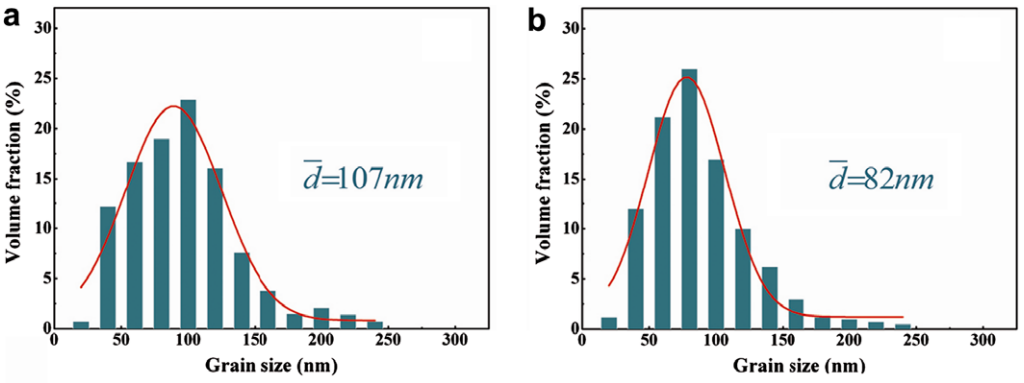

Fig. 4. Statistic grain size of alloys after 4-pass pressing measured by TEM: (a) Cu–5 at.% Al; (b) Cu–8 at.% Al.

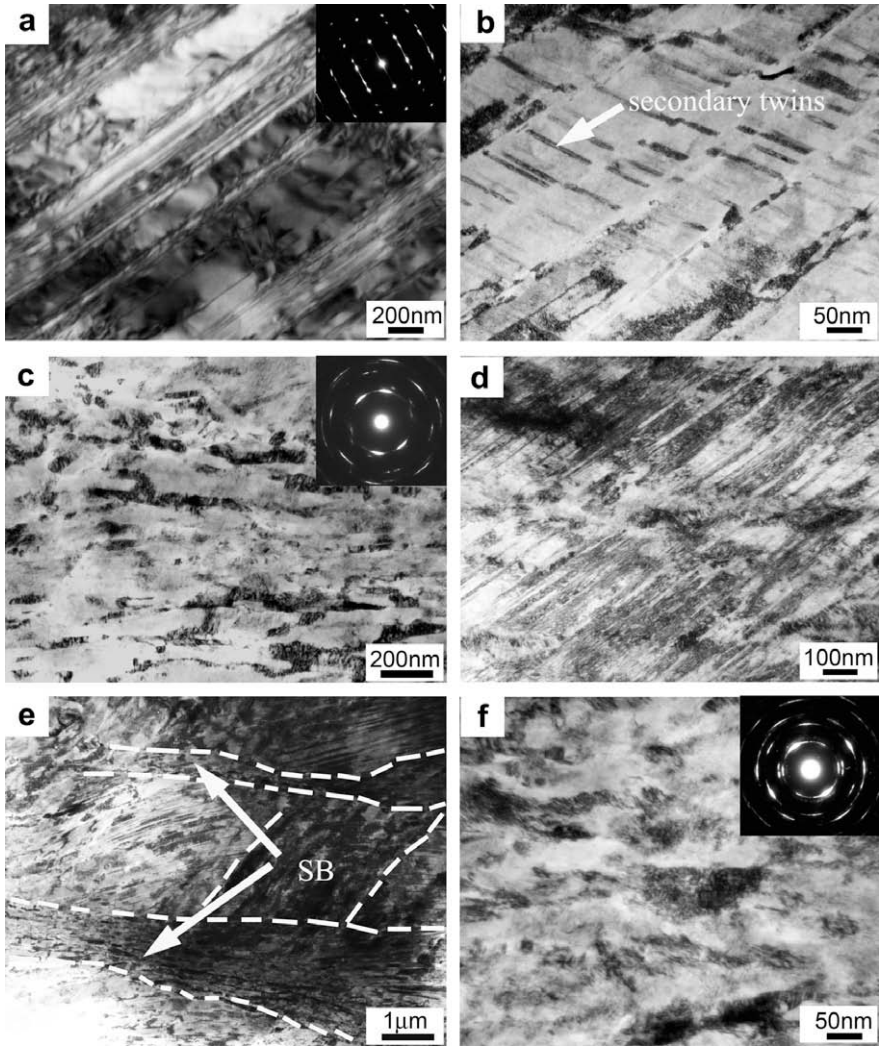

Fig. 5. TEM micrographs of microstructures of CG Cu–16 at.% Al alloy after ECA pressing for: (a–c) one pass; (d–f) two passes.

Cu–8 at.% Al alloy, whose grains are nearly equiaxed. Also, the Cu–8 at.% Al alloy has a somewhat finer grain size (~152 nm) than the Cu–5 at.% Al alloy (~168 nm), both of whose grain sizes were automatically determined by the grain area determination method of the Channel 5 Software, as illustrated in Fig. 7(a) and (c). Thus, the tendency towards homogeneity of microstructures and grain size is consistent with the results obtained by TEM. Nevertheless, the average grain size obtained by the EBSD technique is clearly larger than that detected by TEM. This discrepancy can be due to the different intrinsic resolution ability of the two characterization methods.

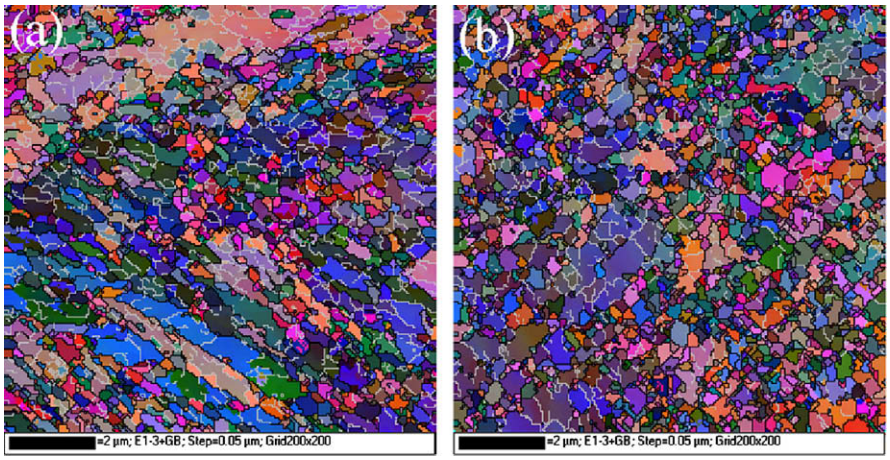

Fig. 6. EBSD maps concerning microstructures of alloys after 4-pass pressing: (a) Cu–5 at.% Al; (b) Cu–8 at.% Al.

The distributions of the misorientation angles in the two Cu–Al alloys are presented in Fig. 7(b) and (d), respectively. It is the large volume fraction of high-angle grain boundaries that powerfully substantiates the formation of the relatively homogeneous fine microstructures after 4-pass ECAP. However, from the statistic data, the corresponding fraction of the high-angle grain boundaries for the ECAPed Cu–5 at.% Al alloy is about 49%, which is essentially lower than that of the ECAPed Cu–8 at.% Al alloy, which is as high as approximately 62% if 15° is considered to be the critical value of high-angle grain boundaries. This difference between the two Cu–Al alloys signals the influence of the refinement mechanism on the effectiveness of grain refinement.

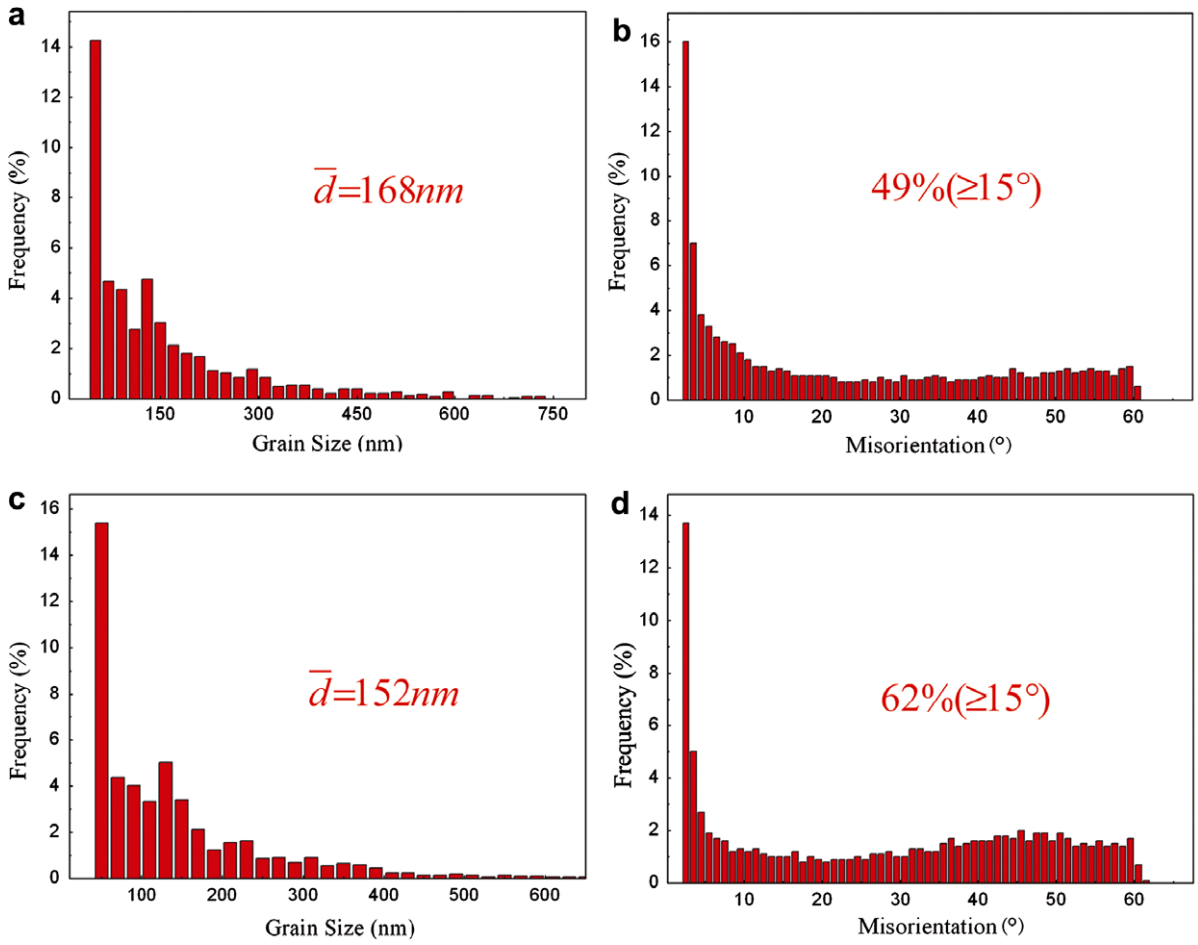

Fig. 7. Misorientation angle and grain size distributions of alloys after 4-pass pressing obtained by EBSD: (a and c) Cu–5 at.% Al; (b and d) Cu–8 at.% Al.

In this work, owing to the limited resolution ability, a scan step of 50 nm made some nanograins and nanoscale twins (below 50 nm) difficult to detect. Thus, it is reasonable to assume, as mentioned above, that the relatively larger grain size obtained by SEM/EBSD can be ascribed to the relatively low resolution compared with TEM, and the distribution of high-angle grain boundaries is also influenced to some extent; meanwhile, the high internal stress of the Cu–Al alloys after 4-pass ECAP also affected the quality of measurements. Notwithstanding this, the general tendency representing grain refinement and the homogeneity of microstructures is apparent, i.e. the equilibrium grain size significantly decreases and the microstructures become more homogeneous by lowering the SFE in Cu–Al alloy under the same processing conditions.

3.3. Tensile properties of Cu–Al alloys after ECAP processes

Fig. 8 shows the tensile engineering stress–strain curves of the three Cu–Al alloys processed from 0- to 4-pass ECAP. The mechanical properties, including yield stress (YS), ultimate tensile stress (UTS) and uniform elongation (UE), as a function of the number of ECAP passes are summarized in Fig. 9 and the corresponding data are listed in Table 1. As shown in the figure and table, strengths, including YS and UTS, are drastically enhanced at the initial deformation stage. With further deformation they slowly increase and approximately reach saturation for specimens subjected to three passes of ECAP. In line with early investigations [1], plastic instability with the onset of necking also occurred during the early stage of tensile deformation in the three Cu–Al alloys after ECAP processes. However, the UE of the processed Cu–Al alloys showed a slight increase with the number of passes, which can be attributed to a smaller decrease in the strain hardening rate Θ as the stress (and strain, respectively) increases [5] (Θ can be defined by $\Theta = (\frac{1}{\sigma}\frac{\partial\sigma}{\partial\varepsilon})_{\dot{\varepsilon}}$ where σ is true stress and ε is true strain). Besides, the elongation to failure is low and nearly remains constant from 10 to 15% over all passes in the three alloys.

More significantly, in parallel with the enhancement in strengths and slight improvement in UE with increasing number of ECAP passes, both strength and UE are simultaneously upgraded by lowering the SFE, as displayed in Fig. 10. Compared with the data in Ref. [5], both the UTS and UE of the ECAPed Cu–16 at.% Al alloy with an SFE of about 6 mJ m^{-2} are nearly twice as large as those of UFG Cu with an SFE of approximate 78 mJ m^{-2}, even though only 2-pass ECAP was applied. This significant improvement in UE caused by lowering the SEF in Cu–Al alloys subjected to the large plastic deformation may originate from the amelioration of the strain hardening rate of specimens. This indicates that the ability of work hardening by the accumulation of dislocations can be regained consequently leading to a larger UE. Therefore, it is reasonable to conjecture that the difference in Θ may be closely related to the influence of the corresponding microstructures of these alloys after ECAP processing.

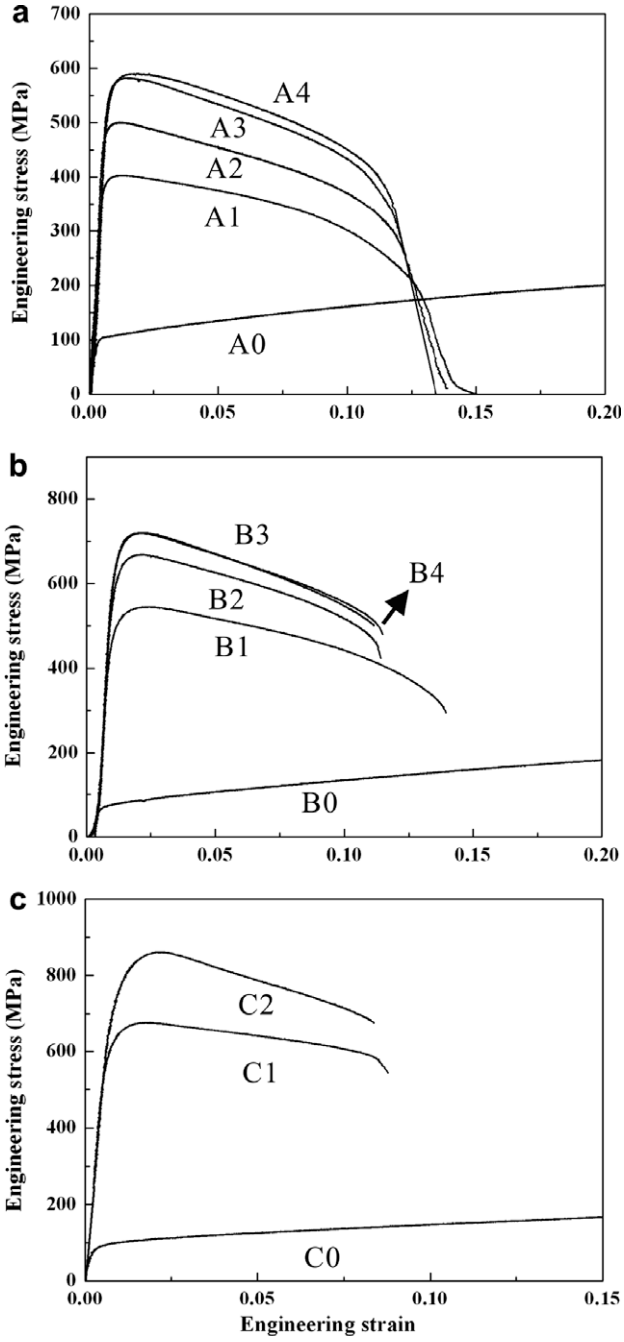

Fig. 8. Tensile engineering stress–strain curves of Cu–Al alloys before and after ECAP: (a) Cu–5 at.% Al (A); (b) Cu–8 at.% Al (B); (c) Cu–16 at.% Al (C). The number (0–4) means the number of ECAP passes.

4. Discussion

4.1. Effect of SFE on microstructures induced by ECAP

An extended screw dislocation is not able to cross slip unless its two partial dislocations recombine into a perfect dislocation; however, this requires energy [29]. The greater

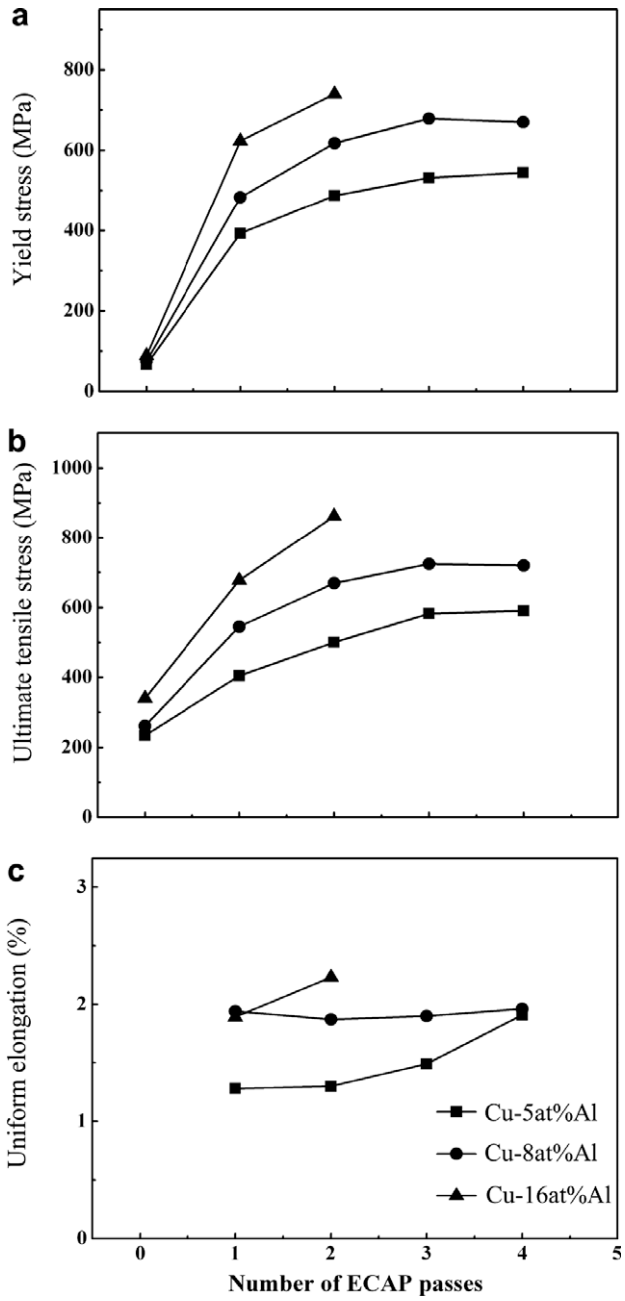

Fig. 9. Mechanical properties of Cu–Al alloys before and after ECAP, including (a) yield stress; (b) ultimate tensile stress; (3) uniform elongation (the data of CG alloys are not shown here).

the width of the SF (the lower SFE) is, the more difficult it is to produce constrictions in it, which will restrict the dislocation activities. Further, cross slip, as an essential dynamic recovery mechanism, plays a crucial role in the rearrangement and annihilation of screw dislocations facilitating the formation of cell-like structures. On the other hand, limited dislocation motion in low-SFE materials restricts the dynamic recovery to form the planar-type dislocation configuration and increases the propensity to form mechanical twins [29]. Thus, owing to the influence of SFE on the dislocation configurations and deformation mechanisms, it must result in the significant difference in the refinement mechanisms, equilibrium grain size and shear bands, which will be discussed separately below.

4.1.1. Refinement mechanisms and microstructural evolution

In the high-/medium-SFE materials, the plastic strain-induced grain refinement is via dislocation manipulation and accumulation [27]. During the early stage of deformation, strong dislocation activities result in the formation of dense dislocation walls or cell walls, and these dislocation configurations subdivide the original coarse grains. With increasing strain, the walls are transformed into sub-boundaries by depositing and recombining more dislocations. The energy and misorientations of sub-boundaries are progressively raised by increasingly generating and annihilating dislocations in the sub-boundaries with further deformation. Consequently, the orientations between grains become fairly random, forming the high-angle boundaries which will be sharpened into conventional grain boundaries through dynamic recovery, and a stabilized grain size is developed as a result of the balance between multiplication and annihilation of dislocations [3–6]. As illustrated in Fig. 2, the grain refinement of Cu–5 at.% Al alloy was predominantly operated by this mechanism. Nevertheless, it is inevitable that, due to its obviously lower SFE than that of pure Cu, some CG grains with proper crystallographic orientations for twinning can be refined through the fragmentations of deformation twins. Because of this, there must be a transition zone in the refinement mechanism from dislocation subdivision to twin fragmentations by lowering the SFE of metals.

In contrast to the metals with high or medium SFE, grain refinement in the materials with low SFE will be predominately operated through twin fragmentations since their deformation involves not only dislocation glide but also deformation twinning. As discussed above, the low SFE will suppress the dislocation motions and, as a result, the deformation twinning becomes increasingly significant in carrying more plastic strain during ECAP. Thus, as shown in Figs. 3 and 5, the formation of the high-density nanoscale twins subdivided the original coarse grains into thin T-M lamellae at the initial stage of the ECAP process in the Cu–8 at.% Al and Cu–16 at.% Al alloys with lower SFE. This is viewed as a crucial step in the easy formation of the subsequent nanostructure. With the further imposition of plastic strain, these lamellae will be "cut" by dislocation activities and intersections of twins [13,23]. It is this "cutting" behavior that transforms 2D T-M lamellae into real three-dimensional nanograins. Therefore, it is reasonable to conclude that the formation of nanometer grains in the Cu–Al alloys with lower SFE is via the fragmentation of these nanoscale twins [13].

In addition, the formation of well-developed shear bands is beneficial to refining the grains, and two kinds of fine grains in these bands were detected: highly elongated nanograins along the shear direction and relatively equiaxed ones obtained through cutting the T-M lamellae, as demonstrated in Figs. 2(c) and 5(f), respectively. And the

Table 1
Tensile properties of three Cu–Al alloys subjected to different passes of ECAP.

	ECAP passes	0	1	2	3	4
Cu–5 at.% Al	YS (0.2%) (MPa)	67	393	487	532	545
	UTS (MPa)	234	403	500	582	590
	Uniform elongation (%)		1.28	1.30	1.49	1.91
Cu–8 at.% Al	YS (0.2%) (MPa)	75	483	618	679	670
	UTS (MPa)	261	545	669	720	722
	Uniform elongation (%)		1.94	1.87	1.90	1.96
Cu–16 at.% Al	YS (0.2%) (MPa)	89	623	740		
	UTS (MPa)	340	694	862		
	Uniform elongation (%)		1.89	2.23		

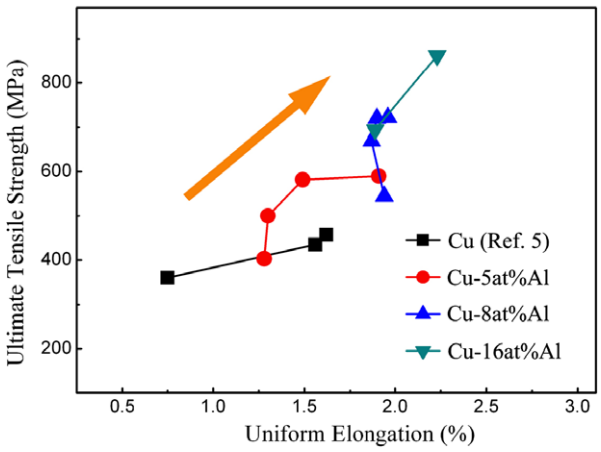

Fig. 10. Relationship between ultimate tensile stress and uniform elongation of CG- and UFG-Cu [5] and Cu–Al alloys with the numbers of pressings, showing the effects of adding Al element and SPD processing on the mechanical properties.

different morphologies of these grains must be due to the distinct types and formation mechanisms of shear bands that are highly influenced by SFE [30], and will be discussed later.

Aside from the refinement mechanism, the microstructure of Cu–8 at.% Al alloy is more homogeneous than that of Cu–5 at.% Al alloy after ECAP for four passes. In addition, it has also been reported that the homogenous microstructure of Al can be achieved after four passes; however, 10 passes is required for the uniform distribution of grain size in Cu [18]. These discrepancies in microstructure evolution may stem from the influence of SFE on the deformation. On the one hand, in comparison with the high-SFE materials, the materials with medium SFE have a lower rate of recovery due to the relatively weak dislocation activities, resulting in a slower evolution of uniform microstructures [18]. On the other hand, deformation twinning transforms homogeneously deformed face-centered cubic (fcc) metals into a laminar fine structure, which will be further divided by the alternating T-M layers and the intersections of twins. These behaviors accelerate the formation of nanograins with a uniform distribution. Nevertheless, under the deformation conditions of ECAP, it is more difficult to form homogeneously twinned structures in medium-SFE metals compared with in low-SFE metals. Consequently, the formation of uniform microstructures is most challenging in the medium-SFE materials. As a conclusion, the homogeneous microstructure of materials with either high or low SFE is much more readily achieved than that of metals with medium SFE when subjected to SPD.

4.1.2. Shear bands

Shear banding is a crucial event of microstructure behavior in fcc metals at large plastic deformation. Its characteristics are determined by many factors, including the method of deformation, strain magnitude, temperature and strain rate, grain size and SFE [30]. According to the values of SFE, two kinds of shear bands can be distinguished and classified into "copper-type" and "brass-type" [30]. The former can always be formed against a background of band-like dislocation structures of elongated cells in high- or medium-SFE materials, as shown in Fig. 11(a); the latter will often be observed in metals with medium-/low-SFE in which the cross slip is suppressed to some extent and deformation twinning becomes an essential deformation mechanism, as displayed in Fig. 11(b). The effects of SFE on the formation and morphology of shear bands have been studied previously [31]: if the SFE is higher, as in the case of Cu [32], the formation of shear bands is delayed; if the SFE is lower, as in the case of Cu–16 at.% Al alloy, shear bands occur at lower strain, all of which have been detected in the present experiments.

The distinct morphologies of two types of shear bands can be ascribed to their different formation mechanisms. In the case of "copper-type" shear bands, this microstructure instability stems from the rigid rotation of the microbands but is not related to the crystalline morphology at very high strain level [32], as illustrated in Figs. 2(c) and 11(a). Meanwhile, in the high-/medium-SFE materials, extensive dynamic recovery can make the boundaries somewhat sharper. In contrast, the origination of "brass-type" shear bands is attributable to the simple rotation of the twinned structure into the observed orientation [30], and evidence of the necessary curvatures of twins were frequently observed in Figs. 3(b) and 11(b). Both kinds of shear bands are initially confined to individual grains; how-

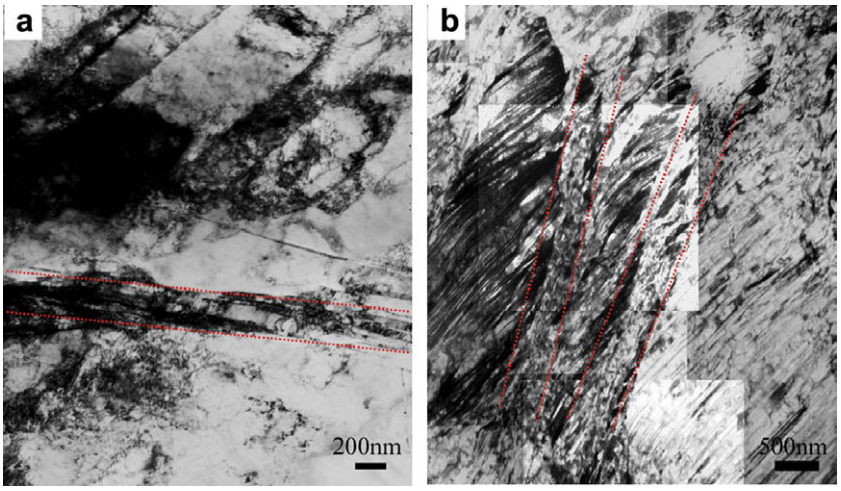

Fig. 11. Typical bright-field TEM images of two types of shear bands formed during the ECAP: (a) copper-type shear bands in the Cu–5 at.% Al; (b) brass-type shear bands in the Cu–8 at.% Al.

ever, they will penetrate grain boundaries or traverse the twinned regions during the later stages of plastic deformation.

For materials with extremely low SFE, macroscopic shear bands (MSBs) readily appear at a high strain level and then traverse the sample during plastic deformation, finally leading to fracture along these MSBs. For example, MSBs were developed during the rolling process, as the strain increased to about 2.1 and 2.8, respectively, in Cu–4.1% Si alloy with an SFE of about 13 mJ m^{-2} and Cu–30% Zn alloy with an SFE of about 15 mJ m^{-2} [32]. Accordingly, it is rational to expect the formation of MSBs to result in the fracture along the main shear plane during the third pass of ECAP pressing with a strain of about 2.3–3.45 in Cu–16 at.% Al alloy with an SFE of about 6 mJ m^{-2}. The formation of these MSBs may arise from the profuse microscale shear bands at high strain level making the volume fraction of the twinned materials insufficient to sustain fresh bands. Thus, with further deformation, these MSBs will propagate across the whole sample, eventually breaking up these materials [32].

4.1.3. Equilibrium grain size

Previous studies have shown that the equilibrium grain size obtained by the plastic deformation-induced refinement is governed by many factors, mainly including the external factors, i.e. loading modes, strain magnitude, temperature and strain rate, and intrinsic factors, e.g. hardness, SFE, melting point, activation energy and bulk modulus [33,34]. During the ECAP processes, there is also a limiting grain size, e.g. ~200 nm for Cu [5,18], ~350 nm for Ni [17] and ~1.3 μm for Al [18], all of whose refinement mechanisms are operated via dislocation subdivision. In the early investigations, it was reported that the equilibrium grain size decreased by lowering the SFE. As shown in Figs. 4 and 7, the minimum grain sizes decrease from the ultrafine-scale to the nanoscale by lowering the SFE of Cu–Al alloys, which is concomitant with the transformation of the refinement mechanism.

Fig. 12 shows the dependence of the normalized limiting grain size, d_{min}/b, on the normalized SFE, γ/Gb, collected from the data reported previously in the fcc metals processed by ECAP, which roughly follows a linear relationship:

$$d_{min}/b = K(\gamma/Gb) \quad (2)$$

where K is a dimensionless parameter ($K = (d_{min}G)/\gamma$), b is Burgers vector and G is the modulus of elasticity in shear (shear modulus) of the corresponding fcc metals. The data are listed in detail in Table 2. Similar relationships between the limiting grain size and SFE were also substantiated in other deformation modes, such as BM [34] and HPT [21,22]. Nevertheless, as exhibited in Fig. 12, comparing the K values obtained by the two different deformation conditions, the K value after ECAP ($K_{ECAP} = 18670$) is remarkably higher than that under HPT ($K_{HPT} = 4950$), whose deformation condition is more rigorous than that

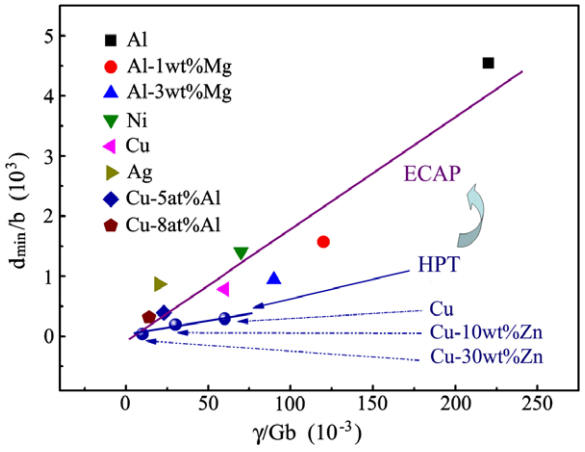

Fig. 12. Normalized equilibrium grain size obtained by ECAP [17,18,35] and BM [34] as a function of the normalized SFE.

of ECAP [22]. This significant distinctness of the slope (K) apparently shows that the dependence of d_{min} on the SFE of materials drastically decreases with increasing degree of severity of deformation conditions. As reported in Ref. [21], under the HPT condition, the grain sizes of metals can be refined down to the nanometer scale; for example, the minimum grain size is ~10 nm for Cu–30 wt.% Zn with an SFE of 14 mJ m^{-2} and ~50 nm for Cu–10 wt.% Zn with and SFE of 35mJ m^{-2}. Even pure Cu with an SFE of 78 mJ m^{-2} can be refined down to ~75 nm, which was achieved by means of SMAT and DPD [12–15]. Because no impurities are introduced by the two methods, the large difference in the limiting grain size of materials processed by ECAP and HPT must stem from the different external processing conditions, including the deformation modes, strain magnitude and strain rate, which also affect the dependence of d_{min} on the SFE of materials. In practice, the grain size of metals with high SFE was also refined down to the nanometer level by using the BM technique, under which the d_{min} shows much less dependence on the SFE than that processed by HPT and ECAP [34]. However, owing to the amount of impurities introduced during processing inhibiting the grain growth, the significantly decreased dependence of d_{min} on the SFE of materials under BM deformation can only be partly attributed to the extremely severe deformation conditions. Therefore, the minimum grain size does decrease by lowering the SFE whatever the external deformation conditions are; however, the dependence of d_{min}/b on γ/Gb, which can be qualitatively reflected by the K value, is determined by the severity grade of external deformation conditions.

4.2. Normalized deformation condition at large strain

It has been widely acknowledged that the microstructure induced by plastic deformation is intrinsically determined by two significant deformation mechanisms: slipping and twinning [29]. The choice of deformation mechanism is predominately governed by the type of material, the SFE and the external loading conditions. Thus, similar to the limiting grain size, the post-deformation microstructures are also essentially influenced by both intrinsic and external factors.

In cubic metals, the intrinsic parameter determining the choice of deformation mechanism most is the value of the SFE. In the materials with a low SFE, the confinement of cross slip makes it insufficient to accommodate plastic deformation by dislocation slip alone; accordingly, deformation twinning can generally occur. As displayed in Fig. 13, as an evident indictor of twinning propensity, the twin fault possibility β, defined as the probability of finding a twin boundary between any two neighboring {1 1 1} planes, can be markedly enhanced with the decrease in SFE of metals or alloys [36,37]. Alternatively, increasing the strain rate and/or lowering the temperature will restrict the dislocation motion and increase the critical resolved shear stress more for slipping than for twinning. As a result, deformation twinning will be the prominent mechanism to carry plastic deformation, even in materials with a medium SFE (such as pure Cu). In fact, the influence of strain rate $\dot{\varepsilon}$ and deformation temperature T on the post-deformation microstructure and mechanical properties can be expressed through a single parameter Z (the Zener–Holloman parameter) [6]:

$$Z = \dot{\varepsilon}\exp\left(\frac{Q}{RT}\right) \text{ or } \ln Z = \ln\dot{\varepsilon} + \frac{Q}{RT} \tag{3}$$

where Q is the activation energy for diffusion [6]. From the equation, it can be that increasing $\dot{\varepsilon}$ and/or lowering T causes an increase in $\ln Z$. As exhibited in Fig. 13, in pure Cu, the volume fraction of deformation twins α distinctly increases with increasing value of $\ln Z$ by the DPD method [38]. Consequently, the values of both $\ln Z$ and SFE are extremely crucial for the formation of deformation twins.

Here, grain refinement and microstructures of the low-SFE Cu–8 at.% Al alloy processed by ECAP with an $\ln Z$ of approximately 25 [6] are analogous with those of Cu processed by DPD with an $\ln Z$ of about 66 [38]. Involuntarily, we can presume whether there is a possibility to normalize some factors including external and intrinsic ones, such as $\ln Z$ and SFE, which affect the post-deformation microstructures and grain refinement mechanisms. Previous investigations about the Z parameter concentrated mainly on $\dot{\varepsilon}$ and T in the same materials [6,38]. As a matter of fact, from Eq. (3), the Z parameter was controlled by two kinds of factors: Q is an intrinsic parameter; while $\dot{\varepsilon}$

Table 2
Parameters of fcc metals subjected to ECAP or HPT deformation [17,18,21,26,34–36].

Deformation modes	Metals	d_{min}/b (10^3)	G (GPa)	γ (m J/m^2)	Metals	d_{min}/b (10^3)	G (GPa)	γ (m J/m^2)
ECAP	Al	4.55	26.2	166	Al–1 wt.% Mg	1.57	~25.9	110
	Al–3 wt.% Mg	0.94	~25.7	90	Ni	1.41	76	128
	Cu	0.78	48	78	Ag	0.87	30.3	22
	Cu–5 at.% Al	0.39	~46.9	28	Cu–8 at.% Al	0.31	~46.2	17
HPT	Cu	0.29	48	78	Cu–10 wt.% Zn	0.19	46.5[21]	35
	Cu–30 wt.% Zn	0.04	40.1[21]	14				

The G values of alloys processed by ECAP are approximately evaluated by using the equation $G_{alloy} = G_A \times (1 - f_B) + G_B \times f_B$ [35], where G_A and G_B are the shear modulus of pure metals; f_B is the atomic fraction of component B. The G value of Mg is about 17 GPa [35] and the weight fraction of Mg is nearly equal to the atomic fraction in Al–Mg alloys.

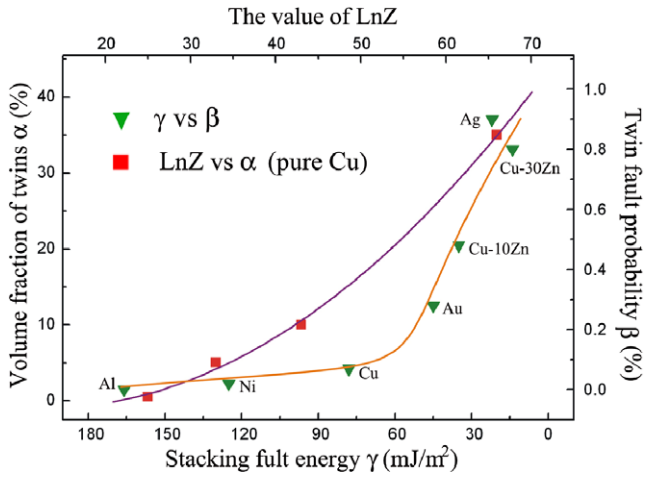

Fig. 13. Two excellent indicators of twinning propensity – twin volume fraction (α) and twin fault possibility (β) – as functions of $\ln Z$ and SFE (γ), respectively, i.e. α vs. $\ln Z$ [38] and β vs. γ [36,37], showing the influence of external deformation conditions and intrinsic properties of materials on the ease of deformation twinning.

and T are highly sensitive to the external conditions. Thus, it can be speculated that changing the SFE could influence the activation energy for diffusion Q, which would make $\ln Z$ under ECAP comparable to that under DPD.

The rate of diffusion as well as the energy required to activate the process can be affected remarkably by the degree of coincidence of grain boundaries [26]. General grain boundaries constitute a region of lattice distortion, resulting in diffusion along a boundary that becomes more favorable as this distortion increases [26]. However, the diffusion may be delayed for certain boundaries whose atom arrangement is highly regular, such as twin boundaries $\sum = 3$, leading to the enhancement of activation energy for diffusion. Owing to the low SFE, these highly regular boundaries form readily at the initial stage of deformation, enhancing the tendency to raise the activation energy. In other words, lowering the SFE to some extent is equivalent to increasing the activation energy, consequently increasing the value of $\ln Z$. Furthermore, the relationship between the minimum grain size and activation energy for diffusion can indirectly substantiate our speculations by [34]:

$$d_{\min}/b = 112e^{-0.0037Q} \tag{4}$$

This implies that a larger Q may result in a smaller limiting grain size during deformation whilst, as discussed in Section 4.1.3, the limiting grain size decreases by lowering the SFE. Accordingly, this indirect evidence makes our hypothesis about the influence of the SFE on $\ln Z$ relatively rational. In principle, lowering the SFE plays a role analogous to increasing $\ln Z$ in suppressing dislocation activities and enhancing the tendency to substitute twinning for slip.

The influences of both factors on the microstructures after high-strain deformation ($\varepsilon > 2$) is preliminarily summarized in Fig. 14. For the metals with high and (extremely) low SFE, the microstructures after large plastic deformations are basically independent of the external factors. In high-SFE materials, cell-like microstructures and subgrains can be formed by extensive dynamic recovery, with the majority of dislocations residing in the cell walls and the interior of cells remaining fairly dislocation-free, [39]. However, their sizes will be reduced very little at strains above two and the microstructures become stable by the balance between the multiplication and recovery processes above the critical strain ε_{cr} [39]. Consequently, cells and subgrains are the main features in the high-SFE materials. In contrast, profuse deformation twins, SFs, microscale shear bands and their interactions are ubiquitous in low-SFE materials because the dislocations can be readily dissociated into partials to form planar arrays of SFs, leading to the formation of abundant twins [29]. Furthermore, for materials with extremely low-SFE, because they are unable to sustain more fresh microscale shear bands, MSBs are readily formed and traverse the whole sample, resulting in the failure of the materials even under deformation conditions with low $\ln Z$. Nevertheless, the microstructures of medium-SFE materials show a significantly high dependence on external factors. After the fairly mild deformation conditions with low $\ln Z$, due to the relatively strong dislocation activities, their microstructures are similar to those of high-SFE metals. However, the main microstructures, induced by deformation with a high value of $\ln Z$ constricting the dislocation motions, present features that are prominently analogous to those of low-SFE materials. Consequently, the effect of enhancing $\ln Z$ on deformation behavior and microstructures is, to some extent, equivalent to lowering the SFE.

4.3. Effect of SFE on mechanical properties

The present investigations provide further experimental support for the results of Ref. [20] showing that the strength and ductility can be simultaneously enhanced

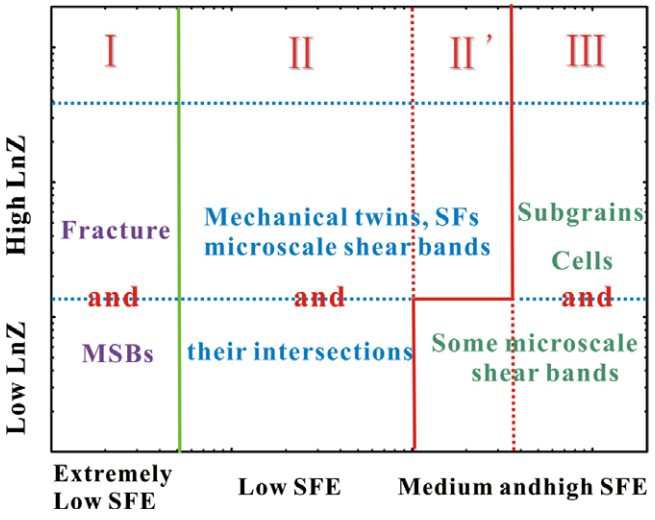

Fig. 14. Illustration of the deformation microstructure map of materials at large plastic strain determined by the relationship between $\ln Z$ and SFE.

through lowering the SFE in Cu–Al alloys. Meanwhile, as expected from Ref. [20], the mechanical properties can be further improved by increasing the number of ECAP passes. In the absence of any effects of the dimensions of specimens on the tensile behavior [40], this simultaneity can be ascribed to the distinct microstructures of these metals processed by ECAP.

The increase in strength produced by lowering the SFE can be readily recognized as the consequence of the formation of profuse SFs, deformation twins and microscale shear bands, and their interactions [41]. Certainly, the solid solution of atoms plays a role in enhancing the strength [29]; however, its influence is negligible compared with the experimental observations. The microstructures containing SFs, deformation twins and shear bands are highly anisotropic and resistant to homogeneous deformation by dislocation glide due to the interactions between moving dislocations and their boundaries. Acting as obstacles, shear bands and twin boundaries block the propagation of slip bands on the intersecting planes and decrease the slip barrier spacing. They further reduce the linear dimensions over which internal stress concentrations can build up: increasing stress is required to stimulate further plastic flow [41]. Moreover, the extent of the increase in strength can also be ascribed to the formation of deformation twins. In comparison with the Hall–Petch slopes K_S for slip and K_T for twinning [42], it can be found that

$$K_T \cong (1.5-7)K_S \tag{5}$$

which implies that twin boundaries can block the dislocation glide more effectively than the general grain boundaries.

As mentioned above, the improvement of ductility can be attributed to the increase in Θ, which is controlled by two components: a dislocation storage (hardening) component and a dynamic recovery (softening) component, related to dislocation annihilation processes [29]. Enhancing Θ, which can be achieved by increasing the hardening component and restricting the softening components, will help delay the localized deformation and is crucial for ameliorating uniform elongation [43]. During the ECAP process, in low-SFE materials the development of profuse twins and SFs can offer ample room for dislocation storage [44] and suppress dynamic recovery, thereby hindering the annihilation of dislocation [19]. Furthermore, the intersection of twins may be propitious to the further enhancement of the hardening component because it can dramatically inhibit slip on essentially all slip systems, unlike primary twins, which only affect non-coplanar slip systems [45]. Thus, the presence of profuse deformation twins and their intersections can essentially improve Θ; as a result, the ductility is ameliorated. However, in contrast with their role in strengthening materials, microscale shear bands provide few contributions for ameliorating the ductility, since the formation of these shear bands has no significant effect on the strain hardening rate [45]. Therefore, the improvement in ductility with a decrease in SFE mainly stems from the formation of profuse deformation twins, SFs and their extensive intersections. Besides these factors, the grain boundaries derived from the twins fragmentation may be more stable than those formed by dislocation subdivisions. These equilibrium grain boundaries may aid the enhancement of ductility of UFG/NC metals [46]. However, further investigations are needed to validate this speculation.

In combination with the results reported earlier, the relationship between mechanical properties and microstructures is summarized in Fig. 15. Strength can be significantly enhanced by increasing the density of dislocations or grain boundaries using the SPD technique [1]; however, this will inevitably deteriorate the ductility of the materials. In contrast to this trade-off, both the strength and the ductility will be simultaneously upgraded if profuse twins and SFs are introduced by the deformation or grow-in methods [19,20,47,48]. In the present work, the better properties may be obtained through low-temperature annealing to remove the resultant defects formed during ECAP, while an efficient pathway is provided to prepare the materials with superior properties and will be further explored elsewhere [49].

5. Conclusions

In this work, we have applied the ECAP technique to prepare UFG/NC Cu–Al alloys with a wide range of SFEs and systematically evaluated the influence of those SFEs on their microstructures and mechanical properties. The results are summarized as follows.

(1) With the decrease in SFE, a transition of the grain refinement mechanism from dislocation subdivision to twin fragmentation was analyzed. In combination with previous investigations, homogeneous micro-

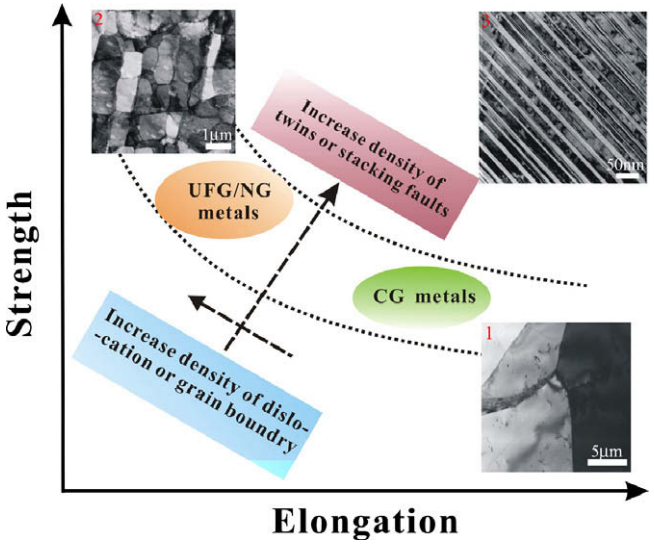

Fig. 15. Relationship between mechanical properties and microstructures of materials processed by various techniques, showing the tendency of simultaneous improvement of strength and ductility through increasing the density of twins and SFs.

structures in materials with a high or low SFE, e.g. Al and Cu–Al alloys, are much more readily achieved than in medium-SFE metals, such as Cu. Several MSBs can be easily formed, resulting in fracture along the main shear plane in materials with an extremely low SFE at large strain.

(2) The grain size of Cu–Al alloys with a low SFE can be refined down to the nanometer scale, validating the fact that the minimum grain size decreased by lowering the SFE. Meanwhile, d_{min}/b roughly fits a linear relationship with the normalized SFE, γ/Gb, and the dependence of d_{min}/b on γ/Gb, qualitatively reflected by the K value, is determined by the degree of severity of external deformation conditions.

(3) Compared with the other deformation modes, lowering the SFE can also enhance the value of $\ln Z$ by changing the intrinsic factors. This can be indirectly substantiated by the relationship between the minimum grain size and the activation energy for diffusion. The factors influencing the microstructure after large plastic deformation were carefully examined. Differing from those of high-/low-SFE materials, which are nearly insensitive to the external deformation conditions, the post-deformation microstructures of medium-SFE materials are highly dependent on them.

(4) The strength and ductility can be simultaneously improved by decreasing the SFE in Cu–Al alloys, which can be attributed to the formation of deformation twins, SFs and microscale shear bands, and their interactions. Combined with the previous results, it can be concluded that the ductility will inevitably be deteriorated only by increasing the density of dislocations and grain boundaries, even though the strength may be greatly enhanced; however, the simultaneous amelioration of strength and ductility can be achieved by increasing the density of twins and SFs through grow-in methods or controlling the SFE of materials.

Acknowledgements

The authors thank Dr. Zhang P., Duan Q.Q., Mrs. Gao W., Mrs. Zhang M.J. and Dr. Han W.Z. for the help of sample pressing, tensile tests, EBSD analysis, TEM observations and stimulating discussions. This work is supported by National Natural Science Foundation of China (NSFC) under Grant Nos. 50571102, 50841024 and 50890173. Zhang Z.F. acknowledge the financial support of the "Hundred of Talents Project" of Chinese Academy of Sciences and the National Outstanding Young Scientist Foundation under Grant No. 50625103.

References

[1] Valiev RZ, Islamgaliev RK, Alexandrov IV. Prog Mater Sci 2000;45:103.
[2] Valiev RZ, Langdon TG. Prog Mater Sci 2006;51:881.
[3] Iwahashi Y, Horita Z, Nemoto M, Langdon TG. Acta Mater 1997;45:4733.
[4] Iwahashi Y, Horita Z, Nemoto M, Langdon TG. Acta Mater 1998;46:3317.
[5] Torre FD, Lapovok R, Sandlin J, Thomson PF, Davies CHJ, Pereloma EV. Acta Mater 2004;52:4819.
[6] Mishra A, Kad BK, Gregor F, Meyers MA. Acta Mater 2007;55:13.
[7] Han WZ, Zhang ZF, Wu SD, Li SX. Acta Mater 2007;55:5889.
[8] Zhilyaev AP, Nurislamova GV, Kim BK, Baró MD, Szpunar JA, Langdon TG. Acta Mater 2003;51:753.
[9] Xu C, Horita Z, Langdon TG. Acta Mater 2007;55:203.
[10] Saito Y, Utsunomiya H, Tsuji N, Sakai T. Acta Mater 1999;47:579.
[11] Liao XZ, Huang JY, Zhu YT. Philos Mag 2003;83:3065.
[12] Zhang HW, Hei ZK, Liu G, Lu J, Lu K. Acta Mater 2003;51:1871.
[13] Wang K, Tao NR, Liu G, Lu J, Lu K. Acta Mater 2006;54:5281.
[14] Li YS, Tao NR, Lu K. Acta Mater 2008;56:230.
[15] Zhang Y, Tao NR, Lu K. Acta Mater 2008;56:2429.
[16] Han BQ, Lavernia EJ, Mohamed FA. Metall Mater Trans A 2003;34:71.
[17] Zhilyaev AP, Kim BK, Szpunar JA. Mater Sci Eng A 2005;391:377.
[18] Komura S, Horita Z, Nemoto M. J Mater Res 1999;14:4044.
[19] Zhao YH, Zhu YT, Liao XZ, Horita Z, Langdon TG. Appl Phys Lett 2006;89:121906.
[20] An XH, Han WZ, Huang CX, Zhang P, Yang G, Wu SD, et al. Appl Phys Lett 2008;92:201915.
[21] Zhao YH, Liao XZ, Zhu YT. Mater Sci Eng A 2005;410:188.
[22] Balogh L, Ungár T, Zhao YH, Zhu YT, Horita Z, Xu C, et al. Acta Mater 2008;56:809.
[23] Huang CX, Yang G, Deng B, Wu SD, Li SX, Zhang ZF. Philos Mag 2007;98:4949.
[24] Jia D, Wang YM, Ramesh KT, Ma E, Zhu YT, Valiev RZ. Appl Phys Lett 2001;79:611.
[25] Wang YM, Chen M, Zhou F, Ma E. Nature 2002;419:912.
[26] Murr LE. Interfacial phenomena in metals and alloys. New York: Addison-Wesley; 1976.
[27] Zhu YT, Lowe TC. Mater Sci Eng A 2000;291:46.
[28] Han WZ, An XH. Unpublished data.
[29] Dieter GE. Mechanical metallurgy. 3rd ed. Boston, MA: McGraw-Hill; 1986.
[30] Paul H, Driver JH, Jasienski Z. Acta Mater 2002;50:815.
[31] Wakefield PJ, Malin AS, Hatherly M. J Aust Inst Met 1977;22:143.
[32] Hatherly M, Malin AS. Met Tech 1979;6:308.
[33] Eckert J, Holzer JC, Krill CE, Johnson WL. J Mater Res 1992;7:1751.
[34] Mohamed FA. Acta Mater 2003;51:4107.
[35] Meyers MA, Chawla KK. Mechanical behavior of materials. Englewood Cliffs, NJ: Prentice Hall; 1999.
[36] Gubicza J, Chinh NQ, Labar JL, Hegedus Z, Cheng X, Langdon TG. Scripta Mater 2008;58:775.
[37] Zhao YH, Liao XZ, Horita Z, Langdon TG, Zhu YT. Mater Sci Eng A 2008;493:123.
[38] Li YS. Ph.D. Thesis, Institute of metal research, CAS, 2008.
[39] Humphreys FJ, Hatherly MM. Recrystallization and related annealing phenomena. Oxford: Elsevier; 2004.
[40] Zhao YH, Guo YZ, Wei Q, Dangelewicz AM, Xu C, Zhu YT, et al. Scripta Mater 2008;59:627.
[41] Christian W, Mahajan S. Prog Mater Sci 1995;39:1.
[42] Meyers MA, Andrade UR, Chokshi AHC. Metall Mater Trans A 1995;26:2881.
[43] Zhao YH, Liao XZ, Cheng S, Ma E, Zhu YT. Adv Mater 2006;18:2280.
[44] Ma E, Wang YM, Lu QH, Sui ML, Lu L, Lu K. Appl Phys Lett 2004;85:4932.
[45] Asgari S, El-Danaf E, Kalidindi SR, Doherty RD. Metall Mater Trans A 1997;28:1781.
[46] Zhao YH, Topping T, Bingert JF, Thornton JJ, Dangelewicz AM, Li Y, et al. Adv Mater 2008;20:3028.
[47] Lu L, Shen Y, Chen X, Qian L, Lu K. Science 2004;304:422.
[48] Chen XH, Lu L. Scripta Mater 2007;57:133.
[49] An XH et al., Unpublished data.